The Journal of Experimental Biology **199**, 717–729 (1996)
Printed in Great Britain © The Company of Biologists Limited 1996
JEB0223

WHY THE URCHIN LOST ITS SPINES: HYDRODYNAMIC FORCES AND SURVIVORSHIP IN THREE ECHINOIDS

MARK DENNY AND BRIAN GAYLORD
Hopkins Marine Station of Stanford University, Pacific Grove, CA 93950, USA

Accepted 15 November 1995

Summary

Two species of sea urchins (*Colobocentrotus atratus* and *Echinometra mathaei*) commonly co-occur on wave-swept intertidal shores in the Indo West Pacific. *E. mathaei* is a typical spiny urchin and is confined to cavities in the rock. In contrast, *C. atratus* has an unusual morphology, in which the spines are much reduced, and is found on substrata fully exposed to wave-induced velocities and accelerations. Previous researchers have suggested that spine reduction may therefore be a morphological adaptation to hydrodynamic forces. However, measurement of the drag, lift and accelerational forces on sea urchins show that the adaptive significance of spine reduction is less straightforward than it initially appears. The reduction in drag in *C. atratus* as compared with that in *E. mathaei* is to a large extent offset by an increase in lift. Instead, the 'streamlined' morphology of *C. atratus* seems best adapted to provide a reduction in the force imposed by water acceleration, thereby making it feasible for *C. atratus* to venture safely into the tumultuous flows of the surf zone.

Key words: sea urchin, *Colobocentrotus atratus*, *Echinometra mathaei*, *Strongylocentrotus purpuratus*, hydrodynamic force, accelerational force, lift, drag, stress, survivorship, wave exposure.

Introduction

Sea urchins are characteristically spiny creatures. The long, often sharp-pointed, spines present on the aboral aspects of the body serve as a deterrent to predators and competitors alike, and are ubiquitous among sea urchins of the order Echinoida. It is noteworthy, then, when a single genus differs uniquely from this norm. Urchins in the genus *Colobocentrotus* have aboral spines that are much reduced in size, to the extent that they form a tiling. The spines around the periphery of the test are long but orally–aborally flattened, and are typically angled down against the substratum to form a 'skirt'. The resulting shape is more reminiscent of a limpet than an urchin (Fig. 1A), and this morphological peculiarity is reflected in the behavior of these urchins. For example, *Colobocentrotus atratus*, the shingle urchin, is typically found in the intertidal zone of wave-swept shores, where it clings to the fully exposed surface of the rocks, moving to forage at high tide (Ebert, 1982).

This life style is in sharp contrast to that of other urchins, in particular to that of the co-occurring echinoid *Echinometra mathaei*. On the same wave-swept shores where *C. atratus* lives fully exposed, *E. mathaei* is confined to cavities and crevices in the rock (Ebert, 1982). *E. mathaei* has a more conventional urchin morphology, with long, sharp spines extending radially from the test (Fig. 1B).

The morphological and ecological contrast between *C. atratus* and *E. mathaei* has long attracted the attention of functional morphologists. Mortenson (1943) speculated that the reduction of spines in *C. atratus* was an adaptation to the presence of extreme hydrodynamic forces, and this possibility was explored by Gallien (1986), who measured in the field the drag imposed on exposed *C. atratus* and *E. mathaei* tests. Gallien found that *E. mathaei* had a substantially higher drag than *C. atratus* and a lower adhesive tenacity. As a result, he calculated that *C. atratus* was at a much reduced risk of dislodgment by wave-induced hydrodynamic forces and proposed that this difference in risk could help to explain both the evolutionary reduction of aboral spines in *C. atratus* and the behavioral confinement of *E. mathaei* to crevices and cavities. The comparison between *C. atratus* and *E. mathaei* would thus seem to provide a straightforward example of structural adaptation.

In this study, we re-examine this conclusion, accounting not only for drag but also for the lift and accelerational forces imposed on urchins. The results show that the reduction in drag afforded by the shingle urchin's morphology is largely offset by an increase in lift. In contrast, the accelerational force on *C. atratus* is only about half that on *E. mathaei*. As a consequence, the effective functional result of the morphological changes in *C. atratus* is primarily to make it possible for this urchin to venture safely into the rapid accelerations of the surf zone.

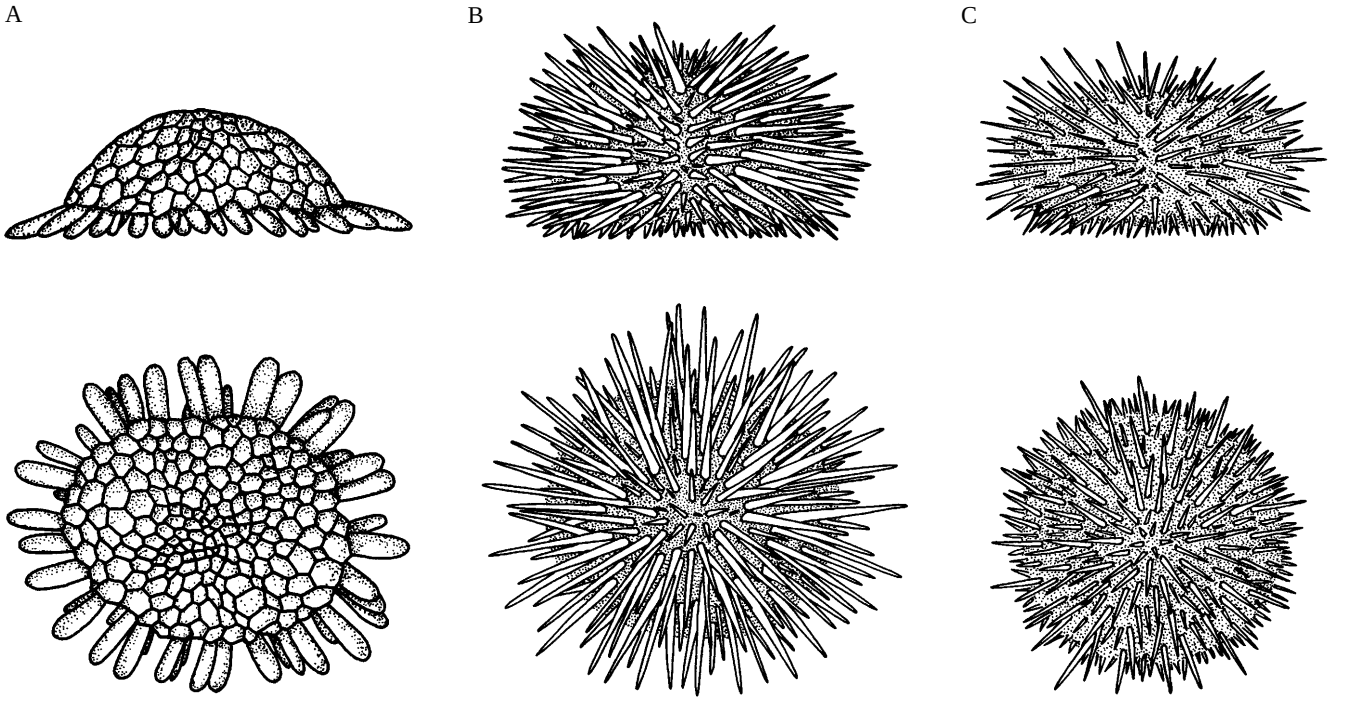

Fig. 1. The urchins used in this study. (A) *Colobocentrotus atratus*, (B) *Echinometra mathaei*, (C) *Strongylocentrotus purpuratus*.

Materials and methods

Species

Colobocentrotus atratus (Linnaeus) and *Echinometra mathaei* (de Blainville) are found commonly through much of the Indo West Pacific (Mortenson, 1943; Ebert, 1982). *C. atratus* is restricted to fully exposed wave-swept shores, while *E. mathaei* is found in both exposed and more protected habitats. On exposed shores, however, *E. mathaei* is found only in microhabitats that afford some protection from wave action (Ebert, 1982). *C. atratus* and *E. mathaei* are closely related, both being members of the subfamily Echinometrinae (Smith, 1988).

A third species is included in this study to serve as a phylogenetic comparison. *Strongylocentrotus purpuratus* (Stimpson), the purple urchin, is found both intertidally and subtidally on moderately and fully exposed rocky shores of the eastern North Pacific from Baja California to Vancouver Island (Morris *et al.* 1980). *S. purpuratus* is in the same family as *C. atratus* and *E. mathaei* (the Echinometridae), but is a member of a different subfamily, the Strongylocentrotinae (Smith, 1988). Like *E. mathaei*, *S. purpuratus* has a typical echinoid shape with long aboral spines (Fig. 1C).

C. atratus and *E. mathaei* were collected on the northern shoreline of the Makapu'u Peninsula (Oahu, Hawaii, 157° 39′ E, 21° 19′ N) from a site seasonally exposed to large waves (Gallien, 1986). The substratum at this site is primarily basalt with some conglomerate inclusions. *S. purpuratus* were collected at Point Arena, California (123° 41.4′ W, 38 ° 54.7′ N), from a site exposed to moderate wave action. The substratum at Point Arena is shale.

C. atratus were relaxed for several hours in a solution of 1 % clove oil in sea water and subsequently dried in their natural posture (Gallien, 1986). *E. mathaei* were placed in an aquarium, covered with a layer of fine sand to hold the spines in a natural position, fixed in place with 10 % buffered formalin, and subsequently dried (Gallien, 1986). *S. purpuratus* were eviscerated immediately after collection and subsequently dried, a procedure that fixed the spines in a natural posture.

Four typical specimens of each species were prepared for measurement of their hydrodynamic force characteristics. The jaw structure was removed from each specimen and a 6 mm diameter metal rod was glued into the resulting cavity to serve as a mount. While the glue set, the orientation of the rod was carefully adjusted so that the axis of the rod was normal to the plane on which the urchin would rest in its natural posture.

The projected area of each specimen was measured along three mutually perpendicular axes: the long axis of the test, the left–right axis (defined to be perpendicular to the long axis) and the oral–aboral axis. Photographs were taken along each axis and digitized (SigmaScan software and a Numonix 2210 digitizing pad). Areas were determined by comparison with a standard included in each photograph. The center of area along each axis was determined by tracing the photograph onto a sheet of paper, carefully cutting out the urchin's outline, and hanging the resulting silhouette from a pin at three or more locations around its perimeter. For each position of the pin, the center of mass of the silhouette (coincident with the center of area) lies vertically below the pin, and this line was traced on the silhouette. The intersection of the lines thus obtained is the center of area.

The volume of each specimen was determined by weighing

the specimen in air and in water to the nearest 0.0001 N. The difference in weight, divided by the acceleration of gravity and the density of water, yields the volume.

Force coefficients

As a practical convenience, drag and lift measurements were conducted in air rather than in water. This transposition of fluids is acceptable provided that the pattern of flow past the organisms is similar between air and water, and this similarity is ensured if the Reynolds number (*Re*) of the flow is the same in the two media (Vogel, 1994). Reynolds number is defined as:

$$Re \equiv \rho u L/\mu\,, \tag{1}$$

where ρ is the density of the fluid (in $kg\,m^{-3}$), u is fluid velocity (in $m\,s^{-1}$), L is a characteristic length (in m) of the object (in this case the length of the organism in the direction of flow) and μ is the dynamic viscosity of the fluid (in $kg\,m^{-1}\,s^{-1}$). Experiments were conducted in a wind-tunnel with a working cross section 28 cm square. A sheet of rugose plastic (a Lego baseplate) 32 cm long by 15 cm wide was held flush to the tunnel wall upstream of the urchin to ensure that the boundary layer was turbulent, as it would be in wave-induced flows in the field. Velocity in the tunnel was varied from 0 to $45\,m\,s^{-1}$, resulting in Reynolds numbers equivalent to those found in sea water at velocities of 0 to approximately $3\,m\,s^{-1}$.

Drag

Drag is a force acting in the direction of flow, caused (at the high Reynolds numbers typical of the wave-swept environment) primarily by an upstream–downstream difference in pressure (Vogel, 1994). To measure drag, an urchin was attached *via* its mounting rod to a circular platform 7 cm in diameter and the platform was held flush with the wall of the wind-tunnel by the drag transducer described by Denny (1989, 1994). The enclosed housing of the transducer prevented the flow of air through the transducer into the tunnel, and the transducer was modified from its previous configuration by the inclusion of a viscous damping device to eliminate any resonant fluctuations of the force platform. The transducer is sensitive to force only along the axis of flow, ensuring that the measurement of drag is not affected by the presence of any lift acting on the specimen.

Drag in the absence of a specimen (essentially the friction drag acting on the mounting platform) was measured, and the drag on each urchin was corrected for the drag acting on the exposed area of the platform. Because the mounting platform is substantially smoother than the natural substratum of urchins, and because the fixed spines of the dry specimens could not be adjusted to fit the substratum precisely, it seemed likely that the space between the oral surface of the urchin and the platform would allow more flow than would the space between the oral surface of a live urchin and a rock. To minimize the effects of such flow, a loose meshwork of cotton wool was placed under each urchin's test (but not the peripheral spines) before mounting on the platform.

The voltage output from the transducer was amplified, low-pass-filtered by a four-pole 25 Hz active low-pass filter, converted to a digital signal, and sampled at 11 Hz. Fifty of these records were averaged to provide a measurement of mean drag at each wind velocity. Mainstream velocity in the tunnel was monitored by a Pitot-static tube as follows. A pressure transducer (Omega PX201A) was coupled to a static port in the tunnel wall. The pressure at the static port was compared with the pressure at a Pitot tube held with its orifice pointed accurately upstream 14 cm from the wall (outside the boundary layer). The difference in pressure between these two ports provides a measure of the dynamic pressure in mainstream flow, from which velocity can be calculated (Vogel, 1994). The voltage output from the pressure transducer was amplified, filtered, digitally recorded and averaged as for the drag transducer.

With a specimen mounted on the drag transducer, the wind velocity was varied in the tunnel. Each pair of averaged drag and averaged wind speed values allowed for a separate calculation of the drag coefficient C_D:

$$C_D \equiv 2F_D/(\rho u^2 A)\,, \tag{2}$$

where F_D is the drag (in N), ρ is the density of air (approximately $1.2\,kg\,m^{-3}$ at 20 °C), u is air velocity (in $m\,s^{-1}$), and A is the projected area (in m^2) along the axis of flow (A_{ap} for flow parallel to the long axis, A_{lr} for flow along the left–right axis). Variation in C_D as a function of the logarithm (base 10) of Reynolds number was estimated for the pooled data from all four specimens of a species using standard least-squares linear regression techniques (Sokal and Rohlf, 1995).

The velocity used in equation 2 is that acting at the level of the center of area for the urchin and orientation in question. This velocity was determined in the absence of a specimen by measurement of boundary layer profiles in the wind-tunnel for the range of velocities used in these experiments. Profiles were measured by setting the Pitot tube at a range of accurately known distances from the tunnel wall, with the results shown in Fig. 2. With the rugose plate upstream from the measurement site, the velocity at a given distance from the wall was a fixed fraction of mainstream velocity, irrespective of the actual magnitude of mainstream velocity. This constancy facilitated the calculation of the effective local velocity for the various urchins, which varied substantially in the location of their center of area.

Lift

Lift is a force acting perpendicular to the direction of flow. As with drag, lift is caused by a difference in pressure between two sides of an organism (Vogel, 1994). Measurements of lift were conducted in separate experiments similar to those for drag except that force was measured perpendicular to the tunnel wall. The lift transducer (similar to that of Denny, 1989) consisted of parallel horizontal aluminum beams (oriented parallel to flow) that supported the urchin *via* its mounting rod, which passed through a small hole in the tunnel wall. Displacement of the beams (proportional to lift) was sensed by

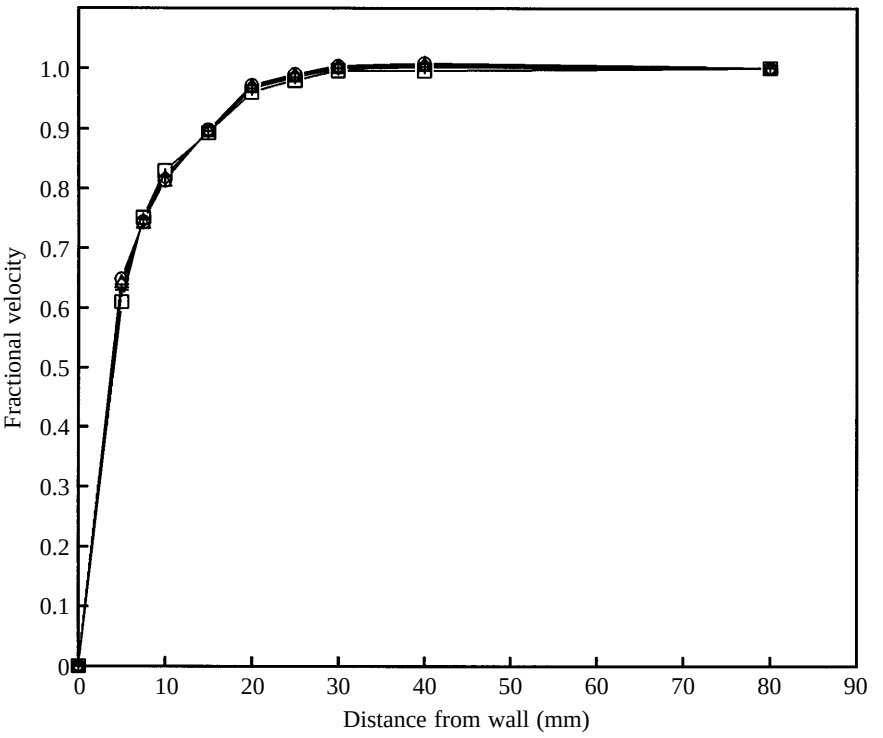

Fig. 2. Wind velocity (expressed as a fraction of mainstream velocity) increases with distance from the tunnel wall. Data are shown for five mainstream velocities (squares, 14.0 m s^{-1}; crosses, 21.4 m s^{-1}; diamonds, 28.9 m s^{-1}; triangles, 36.4 m s^{-1}; circles, 43.9 m s^{-1}).

a linearly variable differential transformer (Schaevitz 100HR), and the beams were viscously overdamped to avoid resonant fluctuations. The relatively large separation between the beams ensured that the transducer was sensitive only to forces perpendicular to the tunnel wall; thus, the lift measurements were not affected by drag.

Specimens were mounted on the lift transducer with their oral side flush against the tunnel wall. As for the drag measurements, a diffuse meshwork of cotton wool was placed between the test and the wall to minimize flow under the test. The force due to the compression of this meshwork contributed negligibly to the recorded lift. For the forces encountered in these tests, the deflection of the transducer's beam (and therefore of the specimen) was less than 0.1 mm, ensuring that displacement of the specimen from the wall would not substantially affect the imposed lift.

Wind velocities and the resulting lift forces were filtered, digitized and averaged as for the drag measurements, and used to calculate the lift coefficient C_L:

$$C_L \equiv 2F_L/(\rho u^2 A_{pl}), \quad (3)$$

where F_L is the lift force (in N) and A_{pl} is the planform area of the urchin (in m^2), the area projected along the oral–aboral axis. Variation in lift coefficient with the logarithm (base 10) of Reynolds number was estimated for a given orientation using the pooled data from all four specimens of a species and standard least-squares regression techniques.

Accelerational force

In addition to lift and drag, which are proportional to the square of water velocity, benthic organisms can be subjected to hydrodynamic forces due to the water's acceleration (Denny *et al.* 1985; Denny, 1988; Gaylord *et al.* 1994). In the case of a stationary organism, these acceleration-dependent forces arise from two sources. First, the pressure gradient driving an accelerating flow produces a 'virtual buoyancy force' in the same way that the vertical pressure gradient created by gravity produces an upward buoyancy force that acts on any object in a stationary water column. This virtual buoyancy force F_b is given by:

$$F_b = \rho V a, \quad (4)$$

where V is the volume of the animal (in m^3) and a is the water's acceleration (in m s^{-2}) relative to the substratum. The second acceleration-dependent force is associated with the local perturbation of flow that occurs in the vicinity of the organism. Establishing a particular pattern of flow around an organism requires an alteration in the momentum of the fluid and, in an accelerating flow where steady state has not been achieved, this change in momentum over time leads to the 'added mass force' F_{am} (Batchelor, 1967):

$$F_{am} = C_a \rho V a. \quad (5)$$

C_a is the added mass coefficient, a dimensionless index that is primarily a function of shape, and the quantity $C_a\rho V$ may be viewed as a mass of fluid that acts, in an inertial sense, as if it were attached to the animal (hence the term 'added mass'). For simplicity, the virtual buoyancy and added mass forces are typically lumped into a single accelerational force F_a:

$$F_a = (1 + C_a)\rho V a, \quad (6)$$

(Denny *et al.* 1985; Denny, 1988; Gaylord *et al.* 1994).

Added mass coefficients for the urchins were measured

using a tow tank in which each specimen was accelerated horizontally through a 3 m long basin of stationary water. A bearing-mounted sled that tracked on polished steel rails was connected *via* a cable and pulley to a 200 kg suspended weight. When dropped, the weight (*via* the gear reduction on the pulley) abruptly accelerated the sled horizontally through the tank at rates of 30–40 m s^{-2}. Peak velocities reached 3 m s^{-1}. Each urchin was attached upside-down to the lower surface of the sled with the urchin's oral surface in the center of, and flush with, the sled's baseplate. This located the urchin approximately 10 cm below the surface of the water and 30 cm above the tank bottom. The baseplate protruded horizontally fore, aft and laterally of the sample to mimic the presence of a flat substratum. The total force acting on each specimen along the axis of travel was measured by a double-beam, cantilever-style transducer, while a second, identical transducer served as an accelerometer by sensing the inertial force. Surface waves (in particular, the bow wave of the sled) were minimized by streamlining all submerged portions of the sled and by setting horizontal plastic plates on the surface of the water in the tank. Cross-wise flow relative to the sample that might otherwise have resulted from movement of water vertically past the lateral edges of the sled was prevented because of the narrow gap between the sides of the tank and the sled's baseplate.

The force and acceleration signals for each run were low-pass-filtered at 50 Hz and recorded digitally at 500 Hz. The acceleration record was then integrated to provide a measure of velocity, and the resulting records of force, acceleration and velocity over time were analyzed as follows to determine the added mass coefficient and the drag coefficient in accelerating flow.

The total force F_{total} recorded for each urchin accelerating through the water was assumed to result from the sum of drag, the accelerational force and an inertial force induced by accelerating both the effective mass of the transducer and the mass of the specimen itself:

$$F_{\text{total}} = F_{\text{D}} + F_{\text{a}} + m_{\text{eff}}a\,, \tag{7}$$

where m_{eff} is the effective mass (in kg) of the transducer plus the mass of the urchin. Substituting from equations 2 and 6 and rearranging yields:

$$F_{\text{total}} = 0.5\rho C_{\text{D}}Au^2 + (1 + C_{\text{a}})\rho Va + m_{\text{eff}}a\,, \tag{8}$$

which can be rewritten as:

$$F_{\text{total}} = \alpha u^2 + \beta a + m_{\text{eff}}a\,. \tag{9}$$

F_{total}, u, a and m_{eff} are known, and equation 9 can be solved for α and β using a least-squares best-fit criterion and an iterative, secant-based method due to Wolfe (1959). The drag and added mass coefficients can then be extracted from α and β.

All tests were conducted for each urchin in each of four orientations: the long axis of the test parallel to flow with either the 'anterior' or 'posterior' end upstream, and the long axis of the test perpendicular to flow with either the 'left' or 'right' side upstream. Here 'anterior' was chosen arbitrarily to refer to one end of the long axis of the test. In the case of *S. purpuratus* (which, having a symmetrical test, has no long axis), a point on the periphery of the test was picked at random, and orientation was expressed relative to this point.

Morphology

The relationships between displaced volume V and (1) total length of the animal along both the anterior–posterior and left–right axes (L and W, respectively), (2) projected area along both the anterior–posterior and left–right axes, and (3) planform area were estimated for each species from values averaged across the four specimens used in the tests. We assume for the sake of simplicity that urchins grow isometrically within the range of sizes relevant to this study; thus, areas are expressed as a function of $V^{2/3}$ and lengths as a function of $V^{1/3}$.

Results

The regression constants for drag and lift coefficients measured in the wind-tunnel are given in Tables 1 and 2, and expected drag and lift coefficients calculated from these data are shown as a function of $\log_{10}Re$ in Fig. 3. The drag coefficient of the shingle urchin *C. atratus* increased slightly with $\log_{10}Re$ for both orientations tested (Fig. 3A). Although the drag coefficient of *E. mathaei* appeared to decrease slightly, the effect was not statistically significant. The drag coefficient of *S. purpuratus* decreased slightly with increasing $\log_{10}Re$. Drag coefficients were compared among urchins at a

Table 1. *Drag coefficients as a function of the logarithm (base 10) of Reynolds number*

	Orientation	B_{D}	M_{D}	r^2	d.f.	P
Colobocentrotus atratus	A–P	0.150	0.098	0.022	375	<0.01
	L–R	0.287	0.085	0.012	337	<0.05
Echinometra mathaei	A–P	0.771	–0.029	0.002	269	NS
	L–R	0.687	–0.006	<0.001	205	NS
Strongylocentrotus purpuratus	–	0.922	–0.057	0.011	604	<0.02

The function used was: $C_{\text{D}}=B_{\text{D}}+M_{\text{D}}(\log Re)$, where C_{D} is drag coefficient, Re is Reynolds number and B_{D} and M_{D} are constants used in the regression equation.

A–P, anterior–posterior axis; L–R, left–right axis.

Table 2. *Lift coefficients as a function of the logarithm (base 10) of Reynolds number*

	Orientation	B_L	M_L	r^2	d.f.	P
Colobocentrotus atratus	A–P	−0.134	0.047	0.097	457	<0.001
	L–R	−0.242	0.085	0.075	476	<0.001
Echinometra mathaei	A–P	−0.020	0.011	0.027	208	0.02
	L–R	−0.021	0.019	0.029	444	<0.001
Strongylocentrotus purpuratus	–	−0.165	0.047	0.298	651	<0.001

The function used was: $C_L=B_L+M_L(\log Re)$, where C_L is lift coefficient, Re is Reynolds number and B_L and M_L are constants used in the regression equation.

Other abbreviations as in Table 1.

Table 3. *Drag coefficients measured in steady and accelerating flow at* Re = 10^5

		Steady flow		Accelerating flow	
	Orientation	C_D	95 % CI	C_D	95 % CI
Colobocentrotus atratus	A–P	0.642	0.020	0.557	0.019
	L–R	0.712	0.027	0.642	0.098
Echinometra mathaei	A–P	0.625	0.016	0.875	0.088
	L–R	0.657	0.024	0.886	0.043
Strongylocentrotus purpuratus	–	0.639	0.008	0.878	0.289

See Table 1 for abbreviations.

typical surf-zone *Re* for these organisms (10^5) and were deemed to be significantly different if there was no overlap in the 95 % confidence intervals about the regression at that value of *Re*. The drag coefficients for flow along the anterior–posterior axis of the test are statistically indistinguishable between *C. atratus* and *E. mathaei* and there are no significant differences between these coefficients and the axis-independent drag coefficient of *S. purpuratus*. The lateral drag coefficient of *C. atratus* is slightly (but significantly) higher than that of the spiny urchins. For an urchin with a flow-wise length of 5 cm, a Reynolds number of 10^5 corresponds to a velocity of 2 m s^{-1} at the level of the urchin's center of area. The difference in drag coefficient between *C. atratus* and the spiny urchins would be accentuated at higher velocities.

Drag coefficients measured in the wind-tunnel (steady flow) were compared with those measured in the tow tank (accelerating flow) (Table 3). In making this comparison, drag coefficients have again been calculated for a Reynolds number of 10^5. The drag coefficients for *C. atratus* broadside to flow are statistically indistinguishable between the wind-tunnel and tow-tank tests, as are the drag coefficients for *S. purpuratus*. The C_D for *C. atratus* with its long axis parallel to flow is slightly smaller in the tow-tank test (0.557 *versus* 0.642),

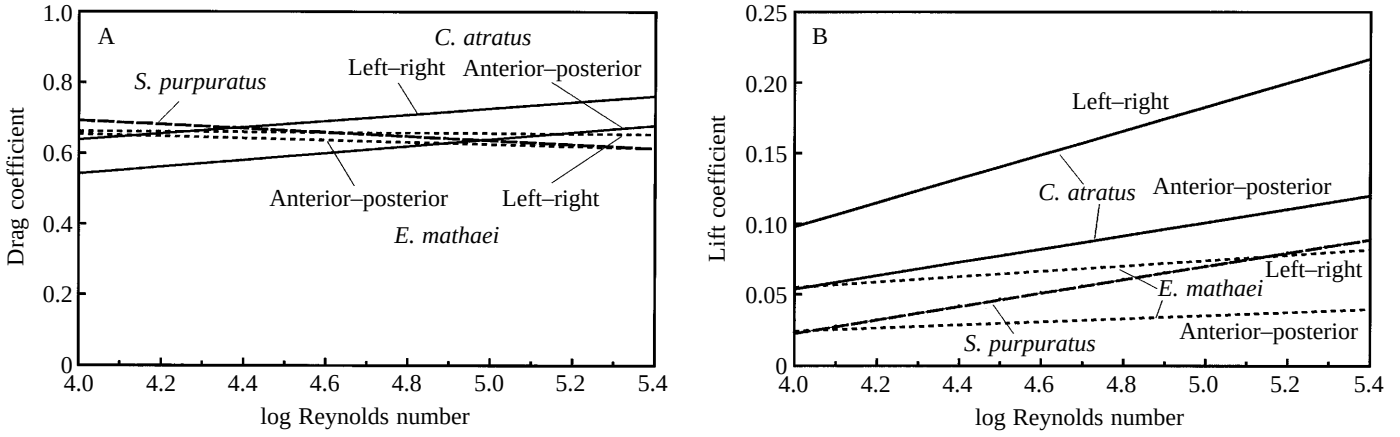

Fig. 3. (A) The variation in drag coefficient with Reynolds number. Lines are the regressions from Table 1. (B) The variation in lift coefficient with Reynolds number. Lines are the regressions from Table 2.

Table 4. *Added mass coefficients for sea urchins*

	Orientation	C_a	S.E.M.	*N*
Colobocentrotus atratus	A–P	0.744	0.039	4
	L–R	0.933	0.102	4
Echinometra mathaei	A–P	2.228	0.295	4
	L–R	2.899	0.166	4
Strongylocentrotus purpuratus	–	1.822	0.386	4

C_a, added mass coefficient.
See Table 1 for other abbreviations.

whereas the values for *E. mathaei* are substantially higher in the tow-tank tests than in the wind-tunnel tests. The reason for the disparity in the *E. mathaei* tests is not readily apparent.

Lift coefficients were compared at a Reynolds number of 10^5, as described above for the drag coefficients. The lift coefficients of *C. atratus* are substantially higher than those of either *E. mathaei* or *S. purpuratus* at all orientations (Table 2; Fig. 3B). For both *C. atratus* and *E. mathaei*, the lift coefficient is significantly higher when the urchin is oriented broadside to flow.

The added mass coefficients of both *E. mathaei* and *S. purpuratus* are significantly and substantially higher than those of *C. atratus* (Table 4).

In summary, the hydrodynamic force coefficients of *E. mathaei*, a typically spiny urchin, are more similar to those of *S. purpuratus*, another spiny urchin but a distant relative, than they are to those of *C. atratus*, a close relative but one with an atypical spine-reduced morphology.

The relationships between body volume and various morphological parameters are given in Table 5. For an urchin of a given volume, *C. atratus* has smaller projected areas (indexed by K_1 and K_2) but a larger planform area (indexed by K_3) than its spiny relatives.

Discussion

These results can be placed in three contexts: (1) the effect of urchin shape on the pattern of flow past the organism, and thus on the force coefficients, (2) the net hydrodynamic force and stress placed on the urchin, that is, the coupling of force coefficients to animal size, and (3) the impact of hydrodynamic forces on urchin survival and behavior. These contexts will be considered in turn.

Force coefficients

Direct measurements of the lift and drag coefficients of *C. atratus* reveal non-intuitive results. Despite the apparent streamlined shape of this echinoderm, its drag coefficient in steady flow is approximately the same as that of the spiny urchins, *E. mathaei* and *S. purpuratus*, and at high Reynolds numbers may be slightly higher (Fig. 3A). Furthermore, at a typical surf-zone velocity, its lift coefficient in a given orientation is more than double that of *E. mathaei* and is substantially higher than that of *S. purpuratus* (Fig. 3B). Thus, the reduction in aboral spine length in this unusual urchin results in a shape that, for a given water velocity and area presented to flow, is actually subjected to larger combined lift and drag forces than that of typical spiny urchins.

In contrast, the added mass coefficient of *C. atratus* is substantially smaller than that of either *E. mathaei* or *S. purpuratus* (Table 4). As a result, if the water's acceleration is sufficiently high, a shingle urchin of a given size may experience a smaller overall hydrodynamic force than a spiny urchin of comparable size, even though *C. atratus* experiences larger lift and drag. If we assume that the evolution of morphology in *C. atratus* has been governed by hydrodynamic effects, comparison of force coefficients suggests an important role for water acceleration rather than water velocity.

Imposed stresses

The surprisingly high drag coefficient of *C. atratus* must be placed in an appropriate context, however. Although the shingle urchin experiences approximately the same drag as that of a spiny urchin for the area it presents to the flow, for a given body volume, the shingle urchin presents much less projected area (Table 5). For example, a shingle urchin of a given volume oriented broadside to flow has only about 54 % the projected area of an *E. mathaei* of the same volume, and

Table 5. *Morphological relationships for the four sea urchins in this study*

	K_1	K_2	K_3	K_4	K_5	*N*
Colobocentrotus atratus	1.183	1.068	4.099	2.725	2.722	4
S.E.M.	0.034	0.040	0.071	0.108	0.044	
Echinometra mathaei	2.234	1.951	3.567	2.577	2.110	4
S.E.M.	0.022	0.108	0.106	0.073	0.071	
Strongylocentrotus purpuratus	1.643	–	3.130	2.159	–	4
S.E.M.	0.097	–	0.139	0.147	–	

A_{ap}, area projected along the anterior–posterior axis of the test; A_{lr}, area projected along the left–right axis; A_{pl}, planform area projected along the oral–aboral axis; *L*, total length (including spines); *W*, total width (including spines).
$A_{ap}=K_1(V)^{2/3}$; $A_{lr}=K_2(V)^{2/3}$; $A_{pl}=K_3(V)^{2/3}$; $L=K_4(V)^{1/3}$; $W=K_5(V)^{1/3}$.

although the area that is presented is subject to approximately the same drag as an equivalent area of spiny urchin, the overall effect is a reduction in drag.

An additional reduction is possible because, owing to its reduced oral–aboral height, a shingle urchin of given volume has a larger fraction of its projected area close to the substratum and, therefore, more of its area is subjected to the reduced velocities of the benthic boundary layer. The extent of this potential reduction in drag is difficult to estimate, however. In the rapid, periodic flows of the surf zone, boundary layers are likely to be quite thin (Denny *et al.* 1985; Denny, 1988), and velocities approaching those in the mainstream may reach within a few millimeters of the substratum. If this is so, the reduction in oral–aboral height in *C. atratus* can yield only a slight reduction in drag. Until precise measurements of the boundary-layer characteristics of surf-zone flows have been measured, however, this conclusion must remain tentative.

As noted above, the unusual morphology of *C. atratus* results both in an increase in lift coefficient relative to that of spiny urchins (Fig. 3B) and in an increase in planform area for an urchin of a given volume (Table 5). As a result, some of the reduction in drag due to the reduction in lateral projected area is offset by an increase in lift. The extent of this trade-off can be explored through a calculation of the overall force F_{LD} imposed on an urchin by the combination of lift and drag:

$$F_{LD} = \sqrt{(0.5\rho u^2 C_D A)^2 + (0.5\rho u^2 C_L A_{pl})^2}\,, \qquad (10)$$

where both the projected area (A, either A_{ap} or A_{lr}) and the planform area (A_{pl}) are functions of urchin volume.

Consider the representative case of urchins with the same typical volume ($10^{-5}\,m^3$) exposed to a surf-zone mainstream velocity of $10\,m\,s^{-1}$. The force imposed on *C. atratus* oriented broadside to flow is 31.8 N, while that imposed on *E. mathaei* is 38.1 N. Thus, although the shingle urchin has only 54 % of the projected area (A_{lr}) of its spiny neighbor, it experiences a force that is 84 % as large, the difference being due primarily to lift.

Some of the effect of the relatively large force imposed on *C. atratus* by drag and lift is mitigated by the relatively large planform area of the test, which provides a large area for attachment to the substratum. Expressed as total force per planform area, the stress imposed on an urchin by lift and drag σ_{LD} is:

$$\sigma_{LD} = \left[\sqrt{(0.5\rho u^2 C_D A)^2 + (0.5\rho u^2 C_L A_{pl})^2}\,\right]/A_{pl}\,. \qquad (11)$$

At a velocity of $10\,m\,s^{-1}$, the stress imposed on an individual *E. mathaei* broadside to flow is therefore 23.0 kPa. The comparable value for *C. atratus* is 16.7 kPa, 73 % of that for *E. mathaei*, a somewhat smaller fraction than that for force (84 %).

The combined force of lift and drag on *S. purpuratus* at $10\,m\,s^{-1}$ is 25.5 N, slightly smaller than that imposed on *C. atratus*, a difference due to the lower lift in this spiny urchin. Owing to the relatively small attachment area of *S. purpuratus*, however, the resulting stress is 17.6 kPa, intermediate between those of *C. atratus* and *E. mathaei*.

In summary, the reduction in drag afforded by the reduction in aboral spines in *C. atratus* is, to a large extent, offset by an increase in lift.

What about the force and stress placed on urchins by the acceleration of the water? For a given displaced volume, the accelerational force placed on *C. atratus* oriented broadside to flow is 50 % of that imposed on *E. mathaei*, and, owing to the relatively larger planform area of *C. atratus*, the stress imposed on the shingle urchin is only 43 % of that of its spiny neighbor. The reduction in accelerational force as a result of spine reduction is thus substantially larger than the reduction in drag. The comparable force and stress values for *C. atratus* and *S. purpuratus* are 69 % and 52 %, respectively.

The overall force and stress imposed on an urchin by the combination of lift, drag and the accelerational force are:

$$F_{total} = \sqrt{[0.5\rho u^2 C_D A + (1 + C_a)\rho a V]^2 + (0.5\rho u^2 C_L A_{pl})^2}\,, \qquad (12)$$

$$\sigma_{total} = \left\{\sqrt{[0.5\rho u^2 C_D A + (1 + C_a)\rho a V]^2 + (0.5\rho u^2 C_L A_{pl})^2}\right\}/A_{pl}\,. \qquad (13)$$

This co-dependence of stress on velocity (u) and acceleration (a) is shown in Fig. 4 for urchins with $V=10^{-5}\,m^3$. The pattern is similar among the three species. Although *C. atratus* experiences slightly less stress than the spiny urchins, the difference is surprisingly small given the drastic differences in morphology.

Risk

Ultimately, however, it is not the stress that an urchin experiences that is important in the evolution of test morphology, but rather the risk imposed by this stress. For an urchin in the surf, an important (if not the dominant) risk is dislodgment from the substratum. A dislodged urchin is likely to be severely battered as it is rolled about and will probably be washed downslope until trapped by some concavity in the rock. On many shores, these concavities are inhabited by anemones quite capable of engulfing and digesting fallen urchins. Thus, dislodgment is often tantamount to death. At what risk of dislodgment are *C. atratus*, *E. mathaei* and *S. purpuratus*?

A full analysis of this question would require extensive testing of the adhesive tenacities of these urchins, and complete data are not yet available. A preliminary exploration can be conducted, however, using tenacity data reported in the literature. Gallien (1986) found that *C. atratus* had a mean tenacity of 120.5±33.6 kPa (S.D.) when the urchins were fully adherent to the rock. When these urchins move to graze, they lift their peripheral spines and raise their test from the substratum. In this upright posture, Gallien (1986) measured a reduced tenacity of 54.4±18.1 kPa (S.D.). Both of these tenacities are substantially (and significantly) larger than that

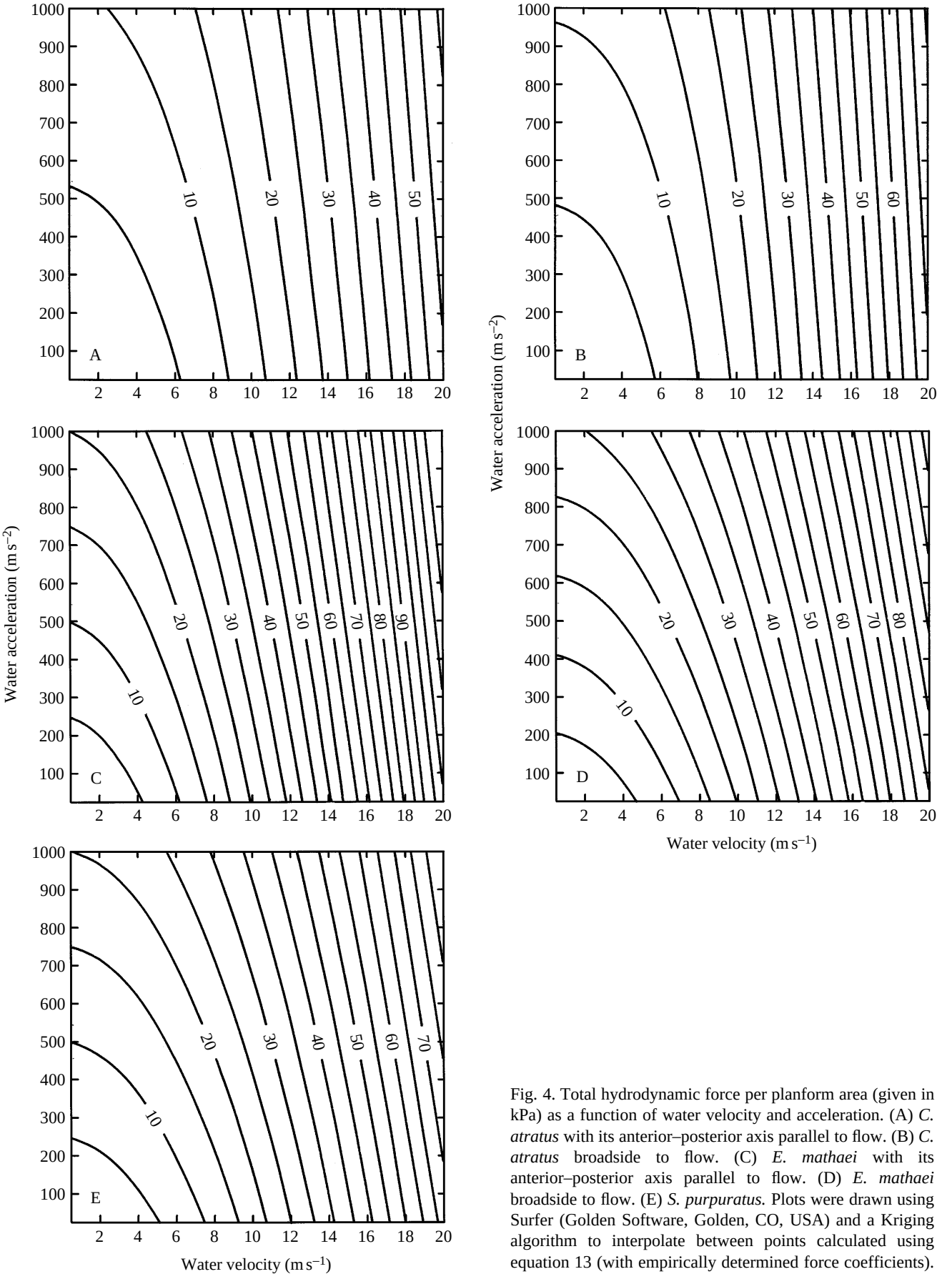

Fig. 4. Total hydrodynamic force per planform area (given in kPa) as a function of water velocity and acceleration. (A) *C. atratus* with its anterior–posterior axis parallel to flow. (B) *C. atratus* broadside to flow. (C) *E. mathaei* with its anterior–posterior axis parallel to flow. (D) *E. mathaei* broadside to flow. (E) *S. purpuratus.* Plots were drawn using Surfer (Golden Software, Golden, CO, USA) and a Kriging algorithm to interpolate between points calculated using equation 13 (with empirically determined force coefficients).

of *E. mathaei*, whose stationary tenacity is 10.3±2.4 kPa (S.D.; Gallien, 1986). The mean tenacity of *S. purpuratus* is intermediate between those of *C. atratus* and *E. mathaei* (38±23 kPa, S.D.; Denny *et al.* 1985).

The tenacities for *E. mathaei* and *C. atratus* were measured for forces applied at a 45 ° angle to the substratum, and that for *S. purpuratus* was measured for force applied parallel to the substratum. The dependence of tenacity on the inclination of force application has not been measured for these urchins, and, lacking these data, we assume that tenacity is independent of the angle of force application.

The precise shape of the probability distribution of tenacities in these urchins is not known, but for present purposes we assume that tenacities are normally distributed about the mean. This assumption seems reasonable given the nature of the adhesive system in urchins, which consists of a multitude of independently suspended tube feet, each with its own suction-cup-and-mucus adhesive organ. The overall adhesion of the urchin, then, is a result of the additive adhesion of many individual tube feet, and while the probability of dislodgment of each tube foot may not be Gaussian, the central limit theorem of statistics (Kendall and Stuart, 1977) suggests that their combined effect should be asymptotically normal.

Given the assumptions of direction-independent and normally distributed tenacities, the probability of dislodgment by the combined effect of water velocity and acceleration can be estimated from σ_{total}, the total stress placed on the urchin by a given flow:

$$\text{Probability of dislodgment} = \int_{-\infty}^{\sigma_{\text{total}}} \frac{1}{s\sqrt{2\pi}} \exp\left[-\frac{(\sigma-\sigma_{\text{avg}})^2}{2s^2}\right] d\sigma. \quad (14)$$

Here, σ_{avg} is the mean tenacity and s is the standard deviation of tenacity.

These probabilities have been calculated for *C. atratus*, *E. mathaei* and *S. purpuratus* with a volume of $10^{-5}\,m^3$ and are shown in Fig. 5. The probability of dislodgment for *E. mathaei* (Fig. 5C,D) increases substantially with any increase in either water velocity or acceleration, and the urchin is at substantial risk of dislodgment even under flow conditions that are relatively benign for exposed, wave-swept shores. For example, if the water's acceleration exceeds 400–500 $m\,s^{-2}$ or its velocity exceeds 7 $m\,s^{-1}$, the urchin has a greater than 50 % chance of being dislodged, and a similar risk is associated with various combinations of lesser acceleration and velocity. The risk of dislodgment for *S. purpuratus* is similar to that for *E. mathaei* (Fig. 5E).

In contrast, the probability of dislodgment in stationary *C. atratus* is low, reaching only 6 % for an urchin caught broadside to flow at a steady velocity of 20 $m\,s^{-1}$, and is virtually independent of acceleration even at accelerations as high as 1000 $m\,s^{-2}$ (Fig. 5A,B). The risk of dislodgment is higher for *C. atratus* in its upright posture (the posture adopted when grazing), reaching approximately 80 % at 20 $m\,s^{-1}$ for an urchin caught broadside to flow (Fig. 6), but is still substantially lower than that of *E. mathaei*. Again, the effect of acceleration on the probability of dislodgment is slight.

The consequences of a reduced added mass coefficient in *C. atratus* are best exemplified by a calculation of the risk to which this spineless urchin would be subjected if it were to have the same tenacity distribution as its spiny neighbor *E. mathaei*. These results are shown in Fig. 7. In this case, the velocity-dependence of the risk is similar for the hypothetical *C. atratus* and the real *E. mathaei* (Fig. 5C,D), but the hypothetical low-tenacity shingle urchin would be capable of surviving much larger accelerations. For example, an acceleration well above 1000 $m\,s^{-2}$ alone (that is, at zero velocity) would be required to dislodge the hypothetical urchin with a probability of 50 %, as opposed to an acceleration of only about 425 $m\,s^{-2}$ required to dislodge 50 % of the real spiny urchins with the same tenacity.

Denny *et al.* (1985) and Gaylord *et al.* (1994) have suggested that the rapid accelerations characteristic of surf-zone flows can limit the effective size to which benthic organisms can grow, a size set by the interplay of applied hydrodynamic forces and the strength of the organism. The larger the organism is, the more young it is likely to produce and the greater its fitness will be. Any increase in size incurs an increase in the risk of dislodgment, however; a result of the disproportionate scaling of strength and the accelerational force. These counteracting factors serve to define a size at which an organism's realized reproductive output is maximized, and this size is often close to that observed in nature (Denny *et al.* 1985; Gaylord *et al.* 1994). By this argument, *C. atratus*, with its low added mass coefficient and high tenacity, could be expected to grow to a larger size than its spiny neighbors. Such is not the case however; *C. atratus* is not noticeably larger than co-occurring *E. mathaei*. The evolutionary 'opportunity' afforded by spine reduction has instead apparently allowed for a shift in the behavior and habitat of this species. Whereas *E. mathaei* is confined to a largely sedentary life in cracks and crevices, *C. atratus* actively forages on exposed substrata.

A calculation of the optimal size of the urchins examined here is possible in theory following the method of Gaylord *et al.* (1994). In practice, however, this calculation must wait until more accurate data are available regarding the precise tenacity distribution of these species and the accelerations present on the shore.

Conclusions and caveats

In the light of these results, the reduction in aboral spine length in *C. atratus* can be placed in a functional context. If *C. atratus* had the same tenacity as its spiny neighbor, the primary consequence of spine reduction in an urchin of a given size would be the ability to withstand higher accelerations. Indeed, accelerations of 400 $m\,s^{-2}$, sufficient in themselves to dislodge a substantial fraction of *E. mathaei*, have been measured in surf (Denny *et al.* 1985), and higher values are suspected to be common. Thus, it seems likely that reduction in spine length in a spiny ancestor of *C. atratus* (separate from any increase

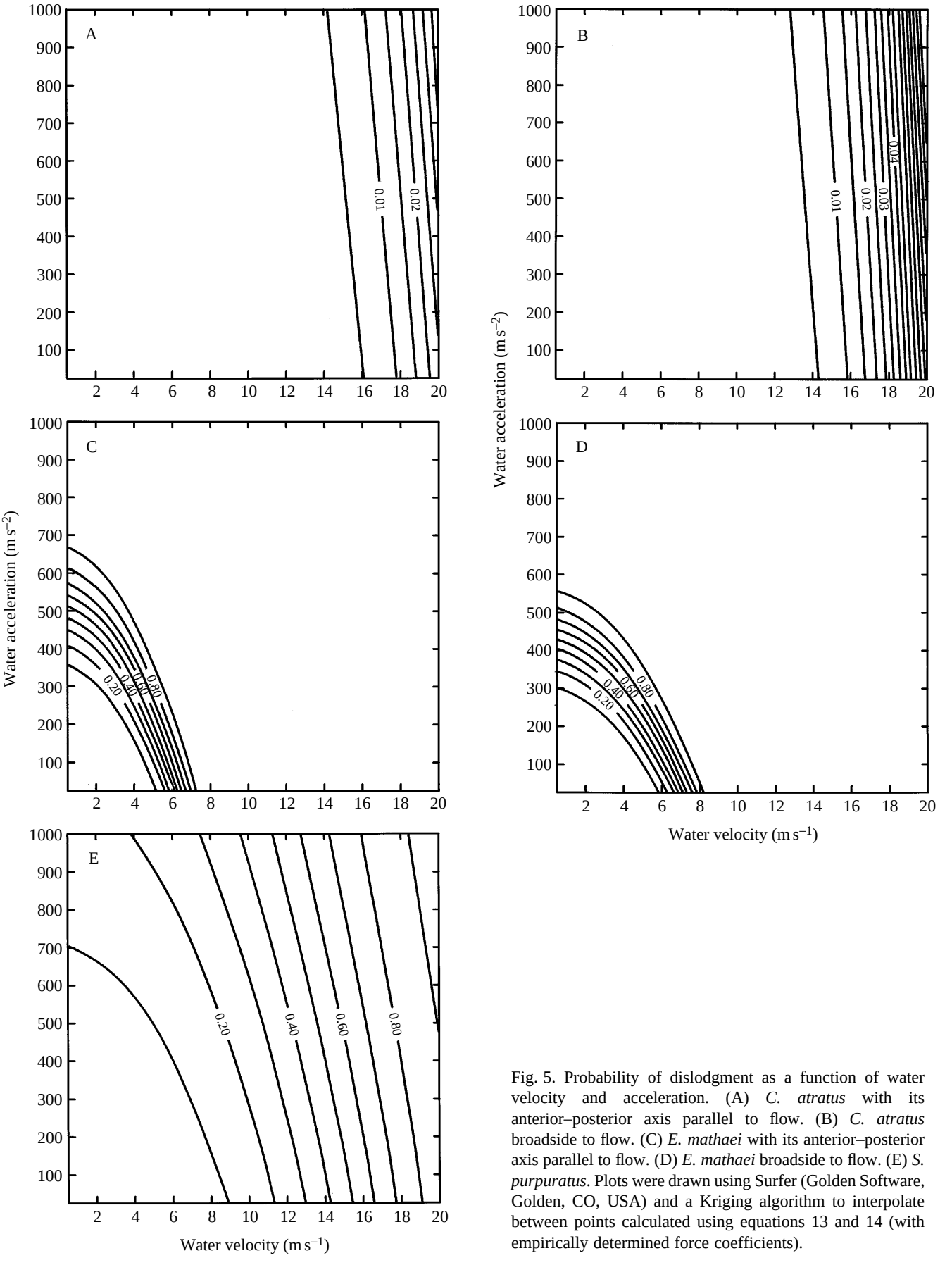

Fig. 5. Probability of dislodgment as a function of water velocity and acceleration. (A) *C. atratus* with its anterior–posterior axis parallel to flow. (B) *C. atratus* broadside to flow. (C) *E. mathaei* with its anterior–posterior axis parallel to flow. (D) *E. mathaei* broadside to flow. (E) *S. purpuratus*. Plots were drawn using Surfer (Golden Software, Golden, CO, USA) and a Kriging algorithm to interpolate between points calculated using equations 13 and 14 (with empirically determined force coefficients).

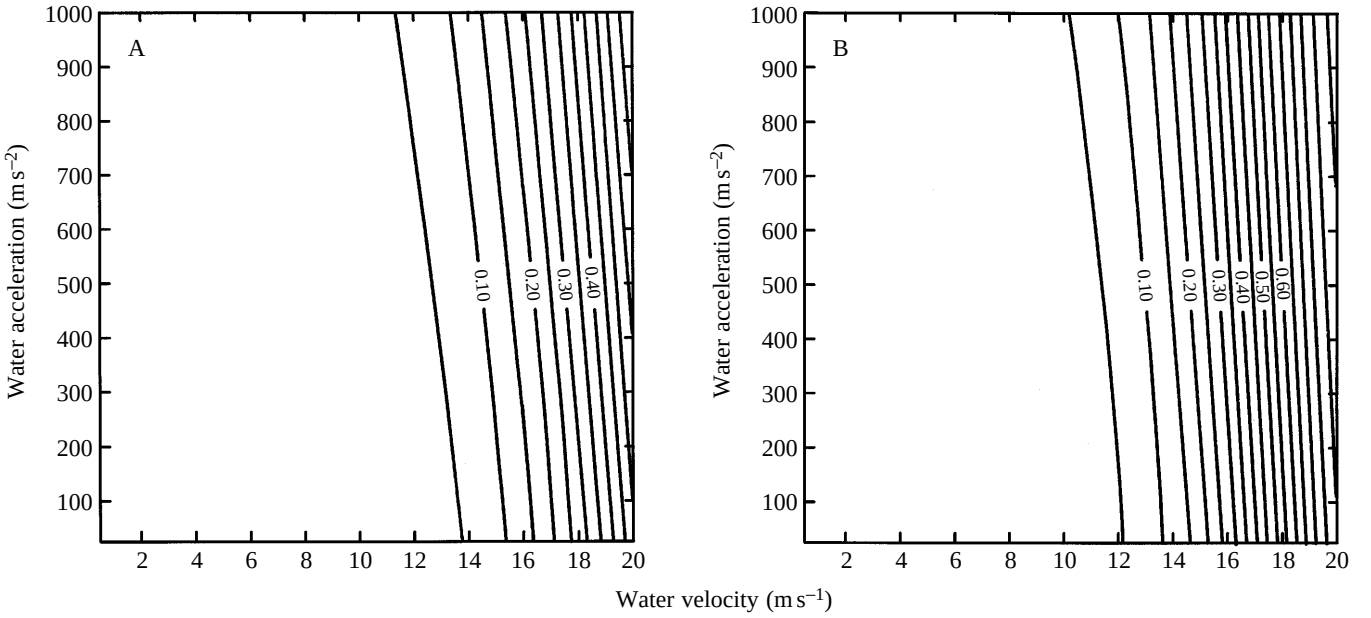

Fig. 6. Probability of dislodgment for *C. atratus* in its upright posture (the posture adopted when grazing). (A) Anterior–posterior axis parallel to flow. (B) Broadside to flow. Plots were drawn using Surfer (Golden Software, Golden, CO, USA) and a Kriging algorithm to interpolate between points calculated using equations 13 and 14 (with empirically determined force coefficients).

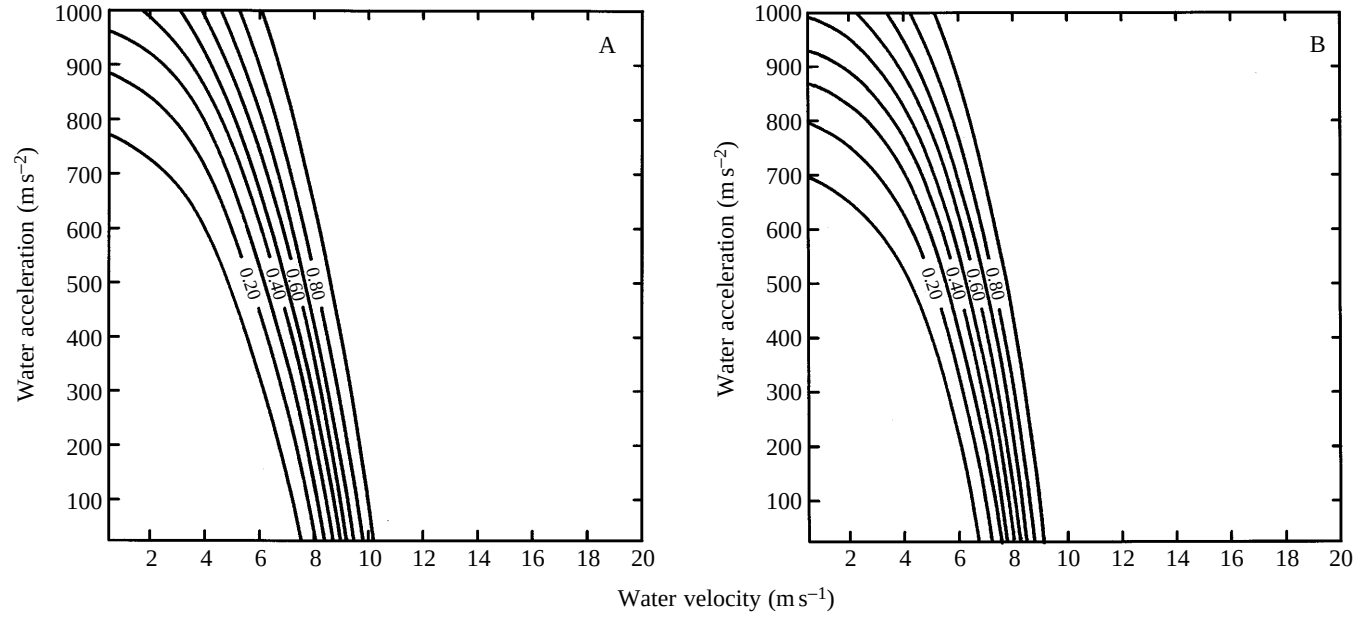

Fig. 7. Probability of dislodgment for a hypothetical *C. atratus* having the same tenacity as *E. mathaei*. (A) Anterior–posterior axis parallel to flow. (B) Broadside to flow. Plots were drawn using Surfer (Golden Software, Golden, CO, USA) and a Kriging algorithm to interpolate between points calculated using equations 13 and 14 (with empirically determined force coefficients).

in tenacity) would allow the urchin to venture into areas of substratum exposed to higher accelerations, that is, to rock surfaces fully exposed to surf-zone flows.

There are two caveats attached to this conclusion. Note first that in Figs 4–7 values of stress and the probability of dislodgment have been calculated for accelerations and equivalent water velocities in excess of those obtained in our empirical measurements of force coefficients. Although substantial shifts in drag coefficients are possible in the range of Reynolds numbers corresponding to these velocities (e.g. an abrupt decrease noted for smooth spheres, cylinders and a limpet; Denny, 1989; Vogel, 1994), this effect seems unlikely for urchins. These shifts in C_D are caused by the transition from a laminar to a turbulent boundary layer and are reduced or

eliminated by even small-scale surface roughness. It thus seems likely that even the relatively regular shape of *C. atratus* would not be subject to an abrupt change in drag coefficient for velocities in excess of those used here. Similar conclusions may be drawn for extrapolations involving the added mass coefficient. Although surf-zone accelerations may reach values substantially larger than those produced in our tow tank, theory predicts that C_a values are a function only of shape and not of acceleration magnitude (Batchelor, 1967). As with all such extrapolations, however, those shown in Figs 4–7 must be viewed as preliminary estimates until empirical data are obtained at higher velocities and accelerations.

Second, by proposing that spine reduction in *C. atratus* may have allowed this urchin to invade portions of the shore that are unavailable to other urchins, we do not suggest that this morphological shift has occurred solely in response to hydrodynamic forces, nor that it occurred without ancillary effects. For example, the invasion of rock surfaces exposed to waves at high tide also exposes *C. atratus* to increased thermal stress and desiccation at low tide. Thus, it is likely that the extant morphology of the shingle urchin represents the evolved response to a variety of environmental factors, and there may be other biological considerations we have not taken into account. It is also clear that spine reduction can be only part of the hydrodynamic story. Much of the ability of *C. atratus* to resist wave-induced forces is due to its unusually high tenacity. Thus, the full story of the functional adaptation of this extraordinary urchin will only be known when further information becomes available regarding its physiology and the mechanism of its high adhesive tenacity.

We thank B. Gallien for the use of his urchins and for bringing these fascinating animals to our attention. F. Sommer kindly lent her artistry to Fig. 1. This study was funded by NSF grant OCE-9115688 to M. D.

References

BATCHELOR, G. K. (1967). *An Introduction to Fluid Dynamics.* Cambridge: Cambridge University Press.

DENNY, M. W. (1988). *Biology and the Mechanics of the Wave-Swept Environment.* Princeton: Princeton University Press.

DENNY, M. W. (1989). A limpet shell shape that reduces drag: laboratory demonstration of a hydrodynamic mechanism and an exploration of its effectiveness in nature. *Can. J. Zool.* **67**, 2098–2106.

DENNY, M. W. (1994). Extreme drag forces and the survivorship of wind- and water-swept organisms. *J. exp. Biol.* **194**, 97–115.

DENNY, M. W., DANIEL, T. L. AND KOEHL, M. A. R. (1985). Mechanical limits to size in wave-swept organisms. *Ecol. Monogr.* **55**, 69–102.

EBERT, T. A. (1982). Longevity, life history and relative body wall size in sea urchins. *Ecol. Monogr.* **52**, 353–394.

GALLIEN, W. B. (1986). A comparison of hydrodynamic forces on two sympatric sea urchins: implications of morphology and habitat. MSc thesis, University of Hawaii, Honolulu, HI, USA.

GAYLORD, B., BLANCHETTE, C. AND DENNY, M. (1994). Mechanical consequences of size in wave-swept algae. *Ecol. Monogr.* **64**, 287–313.

KENDALL, M. G. AND STUART, A. (1977). *The Advanced Theory of Statistics* (4th edn), vol. 1, *Theory of Distributions*. London: Charles Griffin.

MORRIS, R. H., ABBOTT, D. P. AND HADERLIE, E. C. (1980). *Intertidal Invertebrates of California*. Stanford: Stanford University Press.

MORTENSON, T. (1943). *A Monograph of the Echinoida*, vol. 3(3), *Camarodonta* II. Copenhagen: C. A. Reitzel.

SMITH, A. B. (1988). Phylogenetic relationship, divergence times and rates of molecular evolution for Camarodont sea urchins. *Molec. Biol. Evol.* **5**, 345–365.

SOKAL, R. P. AND ROHLF, F. J. (1995). *Biometry* (3rd edn). New York: W. H. Freeman.

VOGEL, S. (1994). *Life in Moving Fluids* (2nd edn). Princeton: Princeton University Press.

WOLFE, P. (1959). The secant method for simultaneous nonlinear equations. *Comm. Ass. comp. Mach.* **2**, 12–13.